Eur. Phys. J. B **17**, 33–42 (2000)

THE EUROPEAN PHYSICAL JOURNAL B

EDP Sciences

Resonance Raman excitation and electronic structure of the single bonded dimers $(C_{60}^-)_2$ and $(C_{59}N)_2$

W. Plank[1], T. Pichler[1,2], H. Kuzmany[1,a], O. Dubay[3], N. Tagmatarchis[4], and K. Prassides[4]

[1] Universität Wien, Institut für Materialphysik, Strudlhofgasse 4, 1090 Wien, Austria
[2] Institut für Festkörper- und Werkstofforschung, 01171 Dresden, Germany
[3] Comenius University, Faculty of Mathematics and Physics, 80 000 Bratislava, Slovakia
[4] School of Chemistry, Physics and Environmental Science, University of Sussex, BN1 9QJ Brighton, UK

Received 25 January 2000 and Received in final form 10 April 2000

Abstract. Raman spectra are presented for the single bonded dimeric fullerene $(C_{60}^-)_2$ and compared to optical spectra and Raman spectra of the isostructural and isoelectronic heterofullerene $(C_{59}N)_2$. The spectra of both materials exhibit strong correlations with respect to splitting, line position, and line intensity. This holds for non resonant excitation with blue and green lasers as well as for the strong resonances observed with red lasers. The latter observation is consistent with a downshift for the electronic transition energies as compared to C_{60}. The absorption edge of thin films of $(C_{59}N)_2$ was found at 1.4 eV. The three intercage modes were observed at 82, 103, and 111, and at 88, 98, and 106 cm^{-1} for $(C_{59}N)_2$ and $(C_{60}^-)_2$, respectively. A surprising difference was found for the position of the pentagonal pinch modes in the two materials as they were observed at 1461 and at 1451 cm^{-1}, for $(C_{59}N)_2$ and $(C_{60}^-)_2$, respectively. This is interpreted as a consequence of some characteristic differences in the electronic structure of the two compounds.

PACS. 61.46.+w Clusters, nanoparticles, and nanocrystalline materials – 63.20.Dj Phonon states and bands, normal modes, and phonon dispersion – 78.30.-j Infrared and Raman spectra

1 Introduction

In the second generation of fullerene research, polymeric structures of the carbon cages on the one hand and special techniques for doping on the other hand have attracted particular attention. One-dimensional, two-dimensional and even three-dimensional polymeric configurations have been prepared in a reasonably large variety. Unfortunately the degree of polymerization is rather uncontrolled except for the lowest possible oligomeric structures where only two monomers are covalently connected. This paper will focus on such dimeric and doped phases.

Classically the doping of fullerenes can proceed by intercalation of strong donors, such as alkali metals, into the structure of the fullerenes. Alternative procedures are the substitution of carbon atoms on the fullerene cage by more electron rich atoms such as nitrogen [1] or by inserting electron donors such as transition metals or rare earth metals into the cage [2]. In the case of doping on the cage with nitrogen, the resulting compound $C_{59}N$ was expected to be a molecular metal as the extra electron should partly fill the empty t_{1u} derived band and thus shift the Fermi level to a position with a finite density of states. However, both early experimental work and quantum-chemical calculations demonstrated that $C_{59}N$ is not stable. It rather undergoes a dimerization reaction to $(C_{59}N)_2$ or a reaction with hydrogen to $C_{59}HN$ [1,3]. Extended quantum-chemical calculations [5] and photoemission experiments [6,7] proved that in the dimeric structure the system is nonmetallic with a gap of 1.4 eV. This gap is about 0.4 eV smaller than the excitonic gap of C_{60}. The connection between the two constituent molecules of the dimer is established by a single C-C bond in a *trans* configuration between C′ carbons on the 6, 6 bond next to the nitrogen in a C_{2h} geometry, as shown in Figure 1a.

Alternative to the substitution of one atom on the cage, doping to a phase with one extra electron was also found to be possible by alkali intercalation at elevated temperatures [8]. In this case the intercalated alkali metal occupies the octahedral lattice site of a *fcc* crystal structure [9]. However, the material turned out not to be stable on cooling but rather to undergo a phase transition to an orthorhombic, polymeric state below about 400 K [10]. The polymer consists of linear chains oriented in the original [110] direction and the C_{60} molecules are connected *via* cyclobutane rings originating from a cyclo addition process. The monomeric structure can be retained at low temperature if the material is rapidly quenched to below 100 K [11]. In this case the structure becomes simple cubic with space group $Pa\overline{3}$ [12]. Warming up yields successively a dimeric state, shown in Figure 1b, an ordered

[a] e-mail: kuzman@ap.univie.ac.at

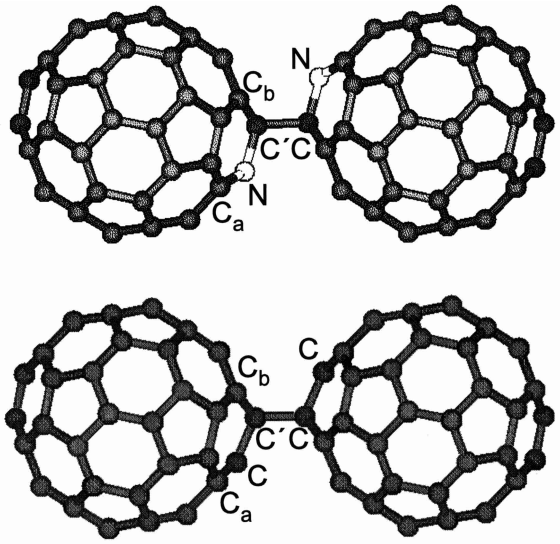

Fig. 1. Molecular configuration for $(C_{59}N)_2$ and for $(C_{60}^-)_2$ as obtained from an AM1 calculation. For both systems the center of inversion is retained. The symmetry of the molecules is C_{2h}.

or disordered monomeric fcc phase, the orthorhombic polymeric phase, and, finally, above 400 K, again the high temperature fcc phase. This sequence of structures was studied with differential scanning calorimetry (DSC) [13,14], electron spin resonance (ESR) [13] and by X-ray analysis [12,15]. Evidence for the single bonded character of the interconnection between the molecule in the dimeric state came from calculations [16] and from structural analysis [17].

Under the above outlined circumstances it is of interest to carry out a comparative study of the two isoelectronic materials, $(C_{60}^-)_2$ and $(C_{59}N)_2$. Raman spectroscopy is expected to be very useful in this case since it probes electronic structures as well as vibrational properties, including symmetry breaking due to distortions of the cage.

The Raman spectrum of the parent material C_{60} is very well understood. The cage has 10 Raman active modes, two of which are nondegenerate and of symmetry A_g and eight are fivefold degenerated of symmetry H_g. The most prominent line originates from the pentagonal pinch mode $A_g(2)$ at 1468 cm^{-1} at room temperature. This line has been widely used to characterize the particular state of the cage as for example the number of charges transferred to it from a donor. As a calibration, a 7 cm^{-1} shift per extra electron is well established, at least for low values of doping. The $A_g(2)$ mode also responds to covalent bonding in the form of a down shift. An even stronger downshift upon charging is known for the mode $H_g(8)$ but splitting of the degeneracy as a consequence of symmetry breaking often hinders the application of this mode for the analysis of the charge transfer. The radial breathing mode $A_g(1)$ at 495 cm^{-1} has been also known to up shift slightly with doping but remains rather stable otherwise. The $H_g(1)$ squashing mode and the $H_g(2)$ mode at 275 and 420 cm^{-1}, respectively, are other well defined species. Both low frequency H_g modes are well known for their splitting upon symmetry reduction. From the previous experience with Raman spectroscopy of charged and polymeric fullerene systems it was necessary to pay particular attention to the behavior of the pinch mode, to characteristic lines at 345 cm^{-1} (or lower), at 625 cm^{-1} and to the intercage modes. A summary of line positions for the important modes of C_{60} in the various phases is listed in the first 5 columns of Table 1. Frequencies are given in cm^{-1}.

We reported recently some details about the Raman spectrum of $(C_{59}N)_2$ [18]. The spectra exhibited a strong resemblance to those of C_{60} but a strong splitting of the lines from the degenerate modes was evident. Also, in some parts of the spectrum the scattering cross section was dramatically enhanced for red laser excitation. This allowed to observe explicitly the three intercage modes around 100 cm^{-1}. Furthermore, the $(C_{59}N)_2$ compound exhibited an unexpected stability which was demonstrated to extend beyond 550 K. This is in dramatic discrepancy to the above described instability of $(C_{60}^-)_2$ which was assigned to a breaking of the intercage bond already below room temperature.

Also, some quenching experiments had been carried out previously in order to observe the vibrational response of the dimeric C_{60} phase [11]. Unfortunately quenching rates at that time were too low to provide single phase material. This seriously hindered the analysis of spectra from the dimers.

In this paper we confirm the characteristic resonance of the Raman spectra from $(C_{59}N)_2$ in the deep red, the response from the intercage modes and the loss of resonance in the IR by exciting the material with several laser lines in the corresponding energy range. The observed resonance is found to be consistent with measurements of the optical absorption. The absorption correlates on the other hand well to results reported from electron energy-loss spectroscopy (EELS) [7]. The development of the various phases established by the C_{60}^- ion are followed in detail and the resonance character of the Raman spectra is demonstrated for this material as well. The splitting of the degenerated modes was found to decrease with decreasing radial character of the modes. The comparison between the two single bonded dimeric systems revealed a very strong similarity but the lines were found to be narrower for the $(C_{60}^-)_2$ dimer. A difference between the two systems was observed for the behavior of the pentagonal pinch mode which is a clear signature for some differences in their electronic configuration.

2 Experiments and geometrical analysis

The biazafullerene samples used in this study were prepared by a chemical route as described previously [18]. For the Raman experiments the powdered material was either loosely pressed into a pellet or drop coated from CS_2 on a gold coated silicon wafer and subsequently again vacuum dried at elevated temperature. Exposition to laser

Table 1. Some relevant frequencies for fullerene dimers in comparison to C_{60} monomers and simple C_{60} polymers. Excitation for the single bonded dimers was with 647.2 or 632.8 nm, lettering for intensities is standard. na: not available, -: phase does not exist, ip: intermediate monomeric phase, cg: center of gravity. Values for the frequencies of $(C_{60})_2$ are from references [19–21].

	C_{60}		C_{60}^-		$(C_{60})_2$	$(C_{60}^-)_2$	$(C_{59}N)_2$
phase	monomer	polymer	monomer	polymer	dimer	dimer	dimer
$H_g(1)$	271	249	273s[a]	249	254w	261s	258s
		256		259	257m	263w	261w
		269		269	267w	270w	267w
		276		275	270m	274s	271s
d293		344		344		293s	288s
$H_g(2)$	432	416	429b[a]	402		415w	420w
		425		412		419w	424m
						425m	427s
		431		431		429w	435w
						434m	437m
d447($G_g(1)$)		452		452		447s	448s
$A_g(1)$, 500 K	495	-	495	-		-	492
270-300 K	496	489	na	490	489s	493s	493s
150-180 K							
80 K			498				491
d513($F_{1g}(1)$)	-	-	-	-	515w	513m	516s
d625($G_g(2)$)						623vs	625m
$A_g(2)$, 500 K	1 465	-	1 457	-	-	-	1 458
270-300 K	1 468	1 459	1 458ip	1 454cg	1 464	1 451	1 463
150-180 K	1 469	1 462	1 462			1 454	1 463
80 K	1 470	1 462	1 463				
$H_g(8)$	1 574	1 563	1 551[a]	1 530	1 574	1 560	1 567cg
		1 577	na	1 559			
intercage							
ν	-	97	-	na	96	88	82
δ_y	-	117	-	na	127	98	103
δ_x	-	173	-	na	139	106	111

[a] at 130 K

radiation was always performed in a vacuum better than 10^{-4} Pa. For the measurement of the optical absorption a thin film of $(C_{59}N)_2$ was deposited under UHV conditions on a single crystal KBr substrate. The deposition process was performed at rather high temperatures (about 800 K) for a total evaporation time of only about 30 minutes to keep the degradation of the material to a minimum. This procedure has been described previously in detail [6]. Raman spectra for the sublimed films proved to be identical to the spectra from the drop coated films.

The dimeric phase of C_{60} was prepared as a thin film on a single crystal in the following way:
a) a single crystal of C_{60} with dimensions of about $3\times3\times2$ mm^3 was heated to 500 K and exposed to Rb vapor in front of the Raman spectrometer. The doping process was monitored by observation of the pinch mode line.

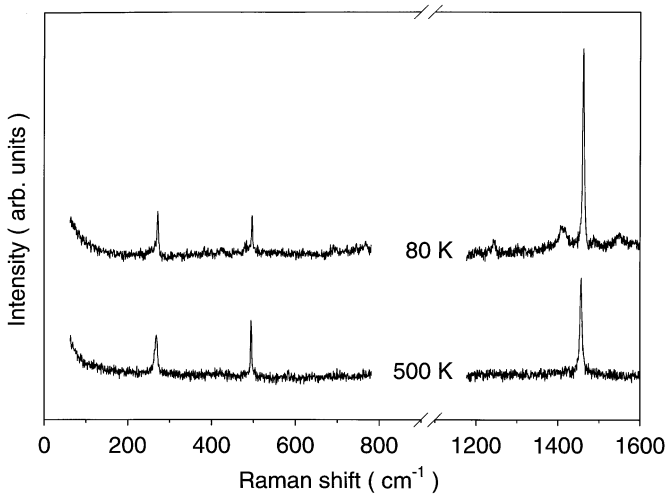

Fig. 2. Low frequency radial and high frequency tangental part of the Raman spectrum of $(C_{60}^-)_2$ as excited with $\lambda = 514.5$ nm before and after quenching.

Overdoping to phase K_3C_{60} or even K_6C_{60} was occasionally observed but these phases could always be dissolved by equilibration at slightly higher temperatures. Finally, even for red laser excitation a spectrum of pure RbC_{60} was observed. During the following sample handling and measurement procedures occasionally a signature of the pentagonal pinch mode from undoped material appeared. Such signatures could always be suppressed by running additional doping-equilibration cycles.

b) The crystal was then rapidly quenched from 500 K to liquid nitrogen temperature. The specially constructed cryostat allowed average quenching rates of about 10 K/s which means 100 K were achieved in about 1 minute. Raman spectra were used to prove the success of the quenching experiment. Figure 2 demonstrates that the high temperature fcc phase was quenched almost completely to the low temperature monomeric compound. The three dominating lines seen are the pentagonal pinch mode (1457/1463 cm^{-1}), the radial breathing mode (495/497 cm^{-1}), and the $H_g(1)$ squashing mode (268/272 cm^{-1}). The numbers give the line positions at high/low temperature, respectively.

c) The crystal was then slowly warmed up until the dimeric phase was observed as it will be demonstrated in detail below. This phase was found to be stable between 160 and 260 K.

d) Finally, the process of warming up was continued until the orthorhombic polymeric phase was obtained just below room temperature.

To learn about the geometrical configuration of the two dimers a semi-empirical AM1 calculation from the MOPAC program was performed with geometry optimization. Results for the geometries are depicted in Table 2 and related to C_{60}. The similarity between the two dimers is evident but intercage bonding appears shorter for $(C_{60}^-)_2$ than that for $(C_{59}N)_2$.

The symmetry analysis of the vibrational modes is identical for the two compounds and summarized in Table 3. The 354 vibrational degrees of freedom are distributed on 91 A_g + 86 B_g + 87 A_u + 90 B_u species where all gerade modes are Raman active and all ungerade modes are IR active. In particular the C_{60} derived degenerated modes H_g, G_g, and F_g splitt into $2A_g + 3B_g$, $2A_g + 2B_g$, and $2A_g + B_g$, respectively. Three of the resulting gerade and ungerade modes each correspond to intercage vibrations which can be determined by reducing the I_h modes of C_{60} to the symmetry C_{2h} of the dimers. As a result we find for both dimers 2 A_g + 1 B_g Raman active intercage modes. A similar distribution of modes is obtained for the IR active modes.

Since the center of inversion is retained for the symmetry group C_{2h} and the number of cage modes is doubled as compared to C_{60} we expect to see all 174 vibrational degrees of freedom from a C_{60} derived cage in the Raman as well as in the IR spectra of the two dimers.

Raman spectra were excited with different laser energies extending from the IR ($\lambda = 1064$ nm) to the blue spectral range and for temperatures between 80 and 500 K. The spectral resolution was 3.5, 3, and 1.5 cm^{-1} for the blue, green and red laser, respectively. Analysis and detection of the scattered light was performed with a Dilor xy spectrometer and with liquid nitrogen cooled CCD detection. Excitation power was limited to less than 0.7 mW with a line focus of 3×0.05 mm^2. To reduce the contamination of the spectra with laser plasma lines the laser beam was purified by a prism monochromator and a line filter. The IR excitation was performed with a Bruker 66v Raman system and a Ge detector with enhanced responsivity. The spectral resolution could not be reduced to below 4 cm^{-1}. With respect to the spectra of $(C_{59}N)_2$ extended use is made from the results reported in [18].

3 Results

3.1 The resonance in $(C_{59}N)_2$

In [18] the pinch mode was found to be downshifted to 1463 cm^{-1} which is much less than expected for one extra electron on the cage and the additional covalent bond. The modes $H_g(7)$ and $H_g(8)$ from C_{60} appear almost unchanged in shape and slightly downshifted to 1425 and 1567 cm^{-1}, respectively. Relevant line positions as they will be needed for the comparison to $(C_{60}^-)_2$ are collected in Table 1, column 8. For the lower H_g modes the situation is very different. $H_g(3)$ and $H_g(4)$, originally at 710 and 780 cm^{-1}, appear strongly split and resonance enhanced in the dimer. At 625 cm^{-1}, a rather strong line appears (at least for excitation with the red laser) which is typical for covalent bonding of cages. Another line which turned out to be crucial for the dimerization is located just above the $A_g(1)$ mode at 516 cm^{-1}. This line often appears as a pair. The components of the $H_g(2)$ mode as they are listed in Column 8 of Table 1 were reassigned as compared to [18]. This reassignment is discussed below.

Table 2. Geometry parameters for $(C_{59}N)_2$, $(C_{60}^-)_2$ and C_{60}. AM1 stands for the semi empirical calculations used in this work. For the C_{60} compounds N must be replaced by C.

AM1	C′−N [Å]	Ca-N [Å]	C′−Cb [Å]	C′−X [Å]	CbC′Cb degrees	CbC′N degrees	NC′X degrees	CbC′X degrees
$(C_{59}N)_2$	1.496	1.446	1.547	1.580	100	113	108	111
$(C_{60}^-)_2$	1.499	1.431	1.546	1.539	100	108	114	112
C_{60}	1.40	1.46	1.46		108			

Table 3. Symmetry and vibrational spectra for single bonded fullerene dimers.

		cage modes		intercage modes	
		R	IR	R	IR
C_{60},C_{60}^-	I_h	$2A_g + 8H_g$	$4F_{1u}$		
$(C_{59}N)$	C_s	$87A'$(IR, R)+$87A''$(IR, R)		-	-
$(C_{60}^-)_2$	C_{2v}	$89A_g + 85B_g$	$85A_u + 89B_u$	$2A_g + B_g$	$2A_u + B_u$
$(C_{59}N)_2$	C_{2v}	$89A_g + 85B_g$	$85A_u + 89B_u$	$2A_g + B_g$	$2A_u + B_u$

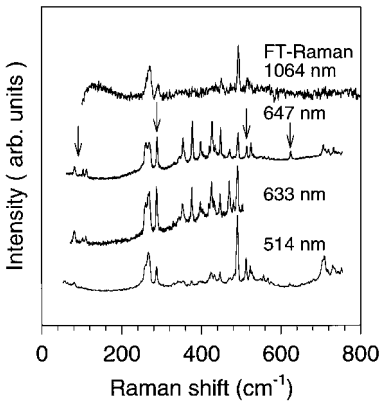

Fig. 3. Raman spectra for the radial cage modes of $(C_{59}N)_2$ for excitation with four different lasers as indicated. The lines most characteristic for the dimer are marked with arrows.

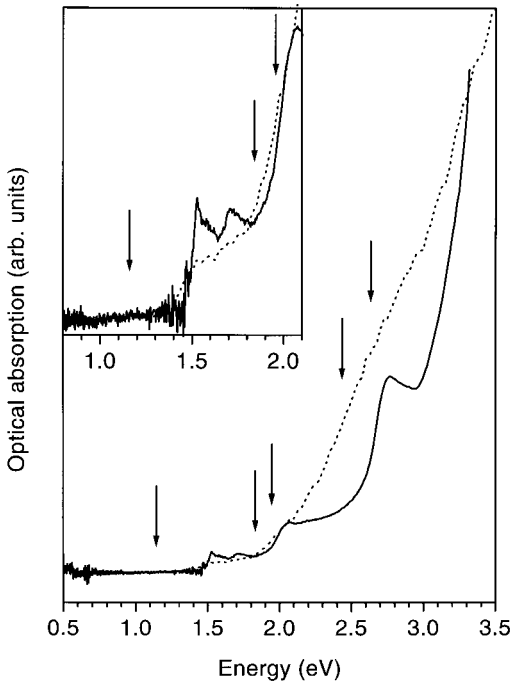

Fig. 4. Optical absorption for $(C_{59}N)_2$. The dotted line is for a thin film on KBr, the full line is for $(C_{59}N)_2$ dissolved in CS_2. The insert depicts a blow up of the edge region. The arrows indicate the positions of the laser lines used for this work.

In order to check the consistency of the dramatic enhancement of the low frequency modes, we studied the low frequency part of the spectrum in more detail by exciting with several red and even IR lasers. The result is demonstrated in Figure 3. Both red laser excitations exhibit the very strong resonance, whereas for the green laser and in particular for the IR laser, the resonance is quenched. The positions of the intercage modes are confirmed for both lasers and their low frequency component appears as a clear feature even for excitation with the green laser, in contrast to the previous results.

The behavior of the resonance is well correlated to the response of the optical absorption. Spectra obtained from a thin film of $(C_{59}N)_2$ on KBr and from $(C_{59}N)_2$ dissolved in CS_2 are depicted in Figure 4. The absorption in the thin film starts just below 1.5 eV but tails down to about 1.3 eV. In solution the cut on of the absorption is even sharper. It starts at 1.4 eV and exhibits several characteristic peaks at 1.5, 1.7, 2, and 2.7 eV. The laser line positions used in this work extend from below the absorption edge to well above. The results for the optical absorption are in good agreement with reports from EELS where a red shift of electronic transition energies was observed as compared to C_{60} [7].

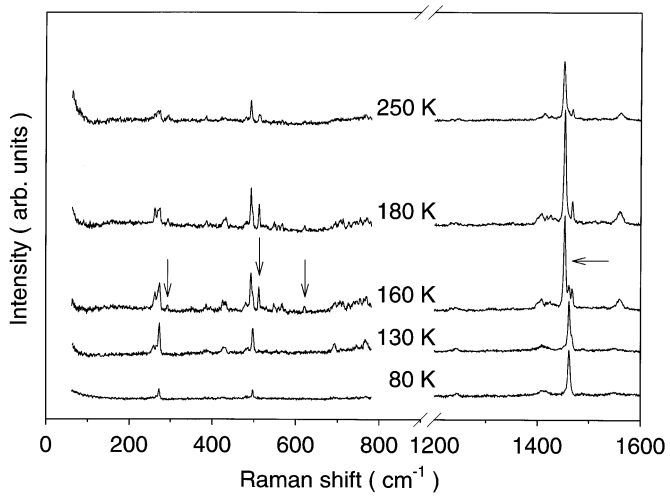

Fig. 5. Raman spectra of quenched $(C_{60}^-)_2$ and for various annealing temperatures. Only the part for the radial modes (left side) and for the tangential modes (right side) is shown. Excitation was for 514.5 nm. Important lines characteristic for the dimer phase are marked with arrows.

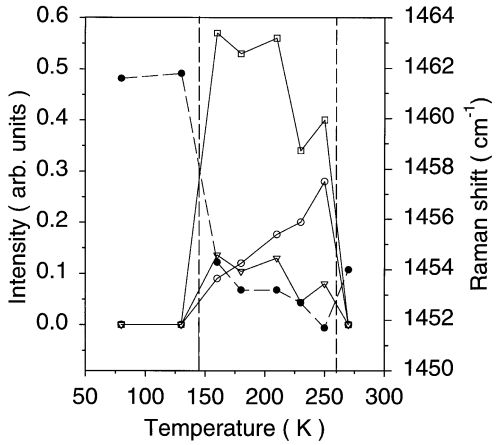

Fig. 6. Transition to the dimeric phase in RbC_{60}. The left scale is for intensities (area) of the modes at 293 (○), 513 (□), and 623 (▽) cm^{-1}, respectively. Intensities relative to the value for the $A_g(1)$ mode were used. The right scale is for the center of gravity of the pinch mode (●). Dashed lines are phase boundaries.

3.2 The phases of RbC_{60}

During the process of warming up, the quenched RbC_{60} single crystal underwent several phase transitions which were followed by their Raman response. Figure 5 depicts the low frequency part of the spectra (left side) and the high frequency part spectra (right side) for selected temperatures between 80 and 250 K as measured with a green laser. The spectra exhibit a characteristic change between 130 and 160 K. New lines appear which can be assigned to the dimer. Such lines are at 293, 513, and 623 cm^{-1}. Also, the two peaks derived from $H_g(3)$ and $H_g(4)$ at 690 and 770 cm^{-1}, respectively, exhibit a spontaneous splitting into many components at 160 K. No intercage modes can be observed under the selected experimental conditions. In the region of the tangential modes the pinch mode is downshifted by 8 cm^{-1}, from 1 462 cm^{-1} to 1 454 cm^{-1}. At 160 K only a very small fraction of the material is left in the monomeric phase. Response from this material is evident from the component in the center of the triplet structure in the pinch mode region of the spectrum. On the other hand, the response from the underlying pristine C_{60} crystal becomes visible.

The transition to the dimeric phase is very sharp as seen in Figure 6 from the plots of the intensities for the various characteristic peaks and the center of gravity for the pinch mode *versus* the sample temperature. The phase transition temperature is just below 150 K where the characteristic dimer lines appear for the first time. Except for small shifts with temperature the line positions for the characteristic peaks remain stable up to 260 K. The intensities for these lines exhibit, on the other hand, varying behavior. The split off component of the $H_g(1)$ mode at 293 cm^{-1} increases rather strongly with temperature, whereas the mode at 513 cm^{-1} drops rapidly until both lines disappear at 270 K where the polymer is developing. The center of gravity for the pinch mode drops suddenly at the phase transition and continues to drop up to 250 K with the usual temperature coefficient of the order of 2 cm^{-1}/100 K. The final rise of the frequency originates from the transition to the polymeric phase.

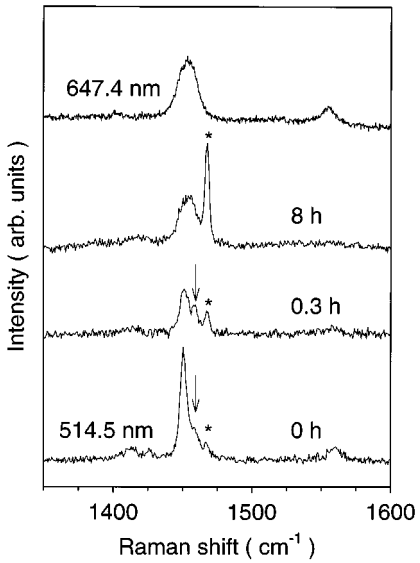

Fig. 7. Behavior of the pentagonal pinch mode of dimeric $(C_{60}^-)_2$ for a crystal exposed to 270 K. Exposure times are indicated in hours. Excitation for the three lower spectra was for 514.5 nm. The lines marked with an asterix originate from underlying C_{60}. The line assigned with an arrow comes from monomeric RbC_{60}. The top spectrum was obtained after reloading the crystal with Rb and for excitation with 647.2 nm.

Beyond 250 K the spectrum starts to change again. Details are best observed in the spectral region of the pinch mode and are demonstrated in Figure 7. The crystal was annealed in front of the spectrometer at a temperature of 270 K for several hours. After 20 minutes

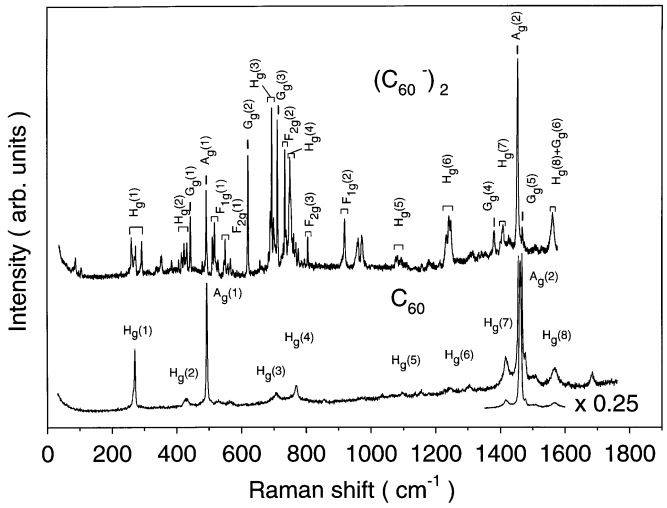

Fig. 8. Raman response for the $(C_{60}^-)_2$ dimer for excitation with 647.2 nm at 180 K in comparison to the response from C_{60} at room temperature. The Mullikan symbols assign the Raman active symmetry species for C_{60} and the C_{60} derived modes for $(C_{60}^-)_2$.

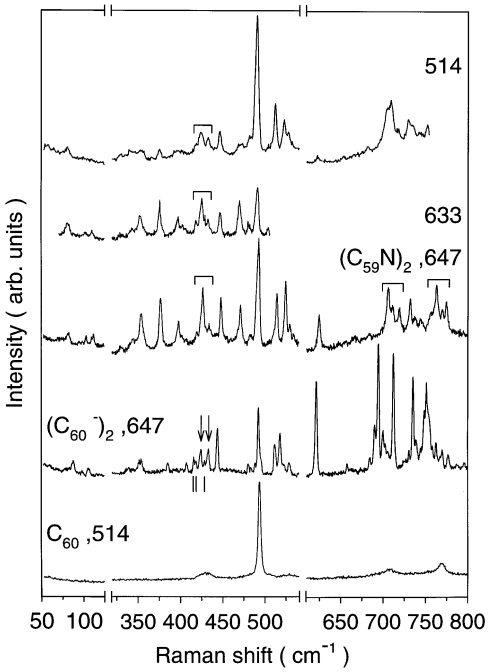

Fig. 9. Raman response for selected regions of the fulleren dimeres $(C_{59}N)_2$, and $(C_{60}^-)_2$ as excited with different lasers as indicated and in comparison to C_{60}; intercage modes (left), $H_g(2)$ and $A_g(1)$ region (center), $H_g(3)$ and $H_g(4)$ region (right).

the response from the dimer was reduced and the line centered at 1 458 cm^{-1} (arrow) appeared. This state was, however, only transient. For extended exposure over 8 hours the system transformed into the polymeric orthorhombic phase as can be seen from the third spectrum in Figure 7. The broad line centered at 1 454 cm^{-1} is characteristic for the latter [22].

The well shaped but rather broad line for the pinch mode from the polymer phase may be expected to originate from a strong disorder in the material. A particular type of disorder can be due to a distribution of chain lengths as it is well known for polymeric systems. In such a case, the shape and position of the line should change for excitation with various lasers. Surprisingly this is not the case for $(C_{60}^-)_2$. The top spectrum in Figure 7 was excited with a red laser after the sample had been reloaded with Rb and reprocessed to avoid the strong response from the underlying C_{60}. Position and shape of the lines excited with the two different lasers are almost identical.

3.3 The resonance in $(C_{60}^-)_2$ in comparison to $(C_{59}N)_2$

Changing the excitation for the Raman spectra of $(C_{60}^-)_2$ from the green to the red results again in a dramatic enhancement of the response as it was observed for $(C_{59}N)_2$. Figure 8 depicts the overall spectrum excited with 647.2 nm at 180 K. Whereas the line positions did not change as compared to the green laser excitation, the intensities increased strongly, particularly in the low and intermediate frequency region. The mode at 623 cm^{-1} (assigned as $G_g(2)$ in the figure) which was one of the markers for the covalently bonded state becomes one of the dominating lines. Its enhancement is about a factor of 20 as compared to the response from the green laser. The response form $H_g(3)$ and $H_g(4)$ becomes particularly strong. The modes appear now as the strongest features in the spectrum. Even the $H_g(6)$ derived features around 1 240 cm^{-1} are enhanced and exhibit a well recognizable splitting. Blowing up the response allowed for the first time to analyze the splitting into five components located at 1 233, 1 235, 1 242, 1 248, and 1 250 cm^{-1}. Only the $H_g(5)$ and $H_g(8)$ modes remain almost unchanged. At the low frequency end of the spectrum the intercage modes appear in a similar pattern to that for $(C_{59}N)_2$.

Relevant modes and their splittings are listed in Table 1 in column 7 in comparison to values for the cyclobutane bonded dimer in column 6. Grouping into splitted species was performed according to the discussion below. The special modes assigned as d293, d457, d513, and d625 were included as obtained from red laser excitation. As already mentioned in the description of the results for $(C_{59}N)_2$, they are very characteristic for the dimeric or polymeric phases. The assignment in the table was based on the same assumptions as used in reference [18], namely that the strongest modes in the dimer originate from the Raman allowed species in C_{60} and the next strongest modes originate from the gerade C_{60} modes. In addition the sequence of species appearing with increasing frequency was adopted from *ab initio* calculations for C_{60}.

Since the resonance enhancement is particularly strong in the low frequency region of the spectrum we have depicted selected parts of it in Figure 9 for resonance conditions, together with the resonance spectrum and the off resonance spectrum for $(C_{59}N)_2$ and C_{60}. As compared

to $(C_{59}N)_2$ the splitting of the individual lines is characteristically smaller for $(C_{60}^-)_2$. For example the lines derived from $H_g(3)$ centered at 690 cm^{-1} and the lines derived from $H_g(4)$ centered at 750 cm^{-1} can be recognized in the latter material whereas they can not be discriminated from other lines in $(C_{59}N)_2$. Also, compared to C_{60} the presentation demonstrates hardly any shift for the centers of gravity of the lines in the case of $(C_{59}N)_2$ but a well expressed shift of about 10 cm^{-1} for the C_{60} dimer.

The strong and narrow line assigned above as d625 is now very well presented and obviously consists of only one component. From the above analysis it is assigned to $G_g(2)$. A line with a similar character can be clearly seen at 712 cm^{-1} for the $(C_{60}^-)_2$ material. It is thus assigned as $G_g(3)$.

These results for $(C_{60}^-)_2$ allow a better assignment for the modes derived from $H_g(3)$ and $H_g(4)$ for $(C_{59}N)_2$. This is indicated in the figure by the two brackets in the spectrum of $(C_{59}N)_2$ excited with 647 nm. Also, the splittings for the doublet on the high frequency side of the radial breathing mode at 493 cm^{-1} is about a factor of two larger in $(C_{59}N)_2$ than in the C_{60} dimer.

The spectral range of the $H_g(2)$ derived modes around 424 cm^{-1} is of particular interest $(C_{60}^-)_2$. Five components are easily recognized. From the relative intensities the two allowed A_g and the three allowed B_g components of the splitted mode can be tentatively identifies as indicated by the arrows and by the lines in the figure. The components are at 415, 419, 425, 429, and 434 cm^{-1}, respectively as listed in Table 1. Comparing this to the results for $(C_{59}N)_2$ requests a reassignment for the $H_g(2)$ derived modes in this material as well. This assignment is used in Table 1.

Finally, the intercage modes for the C_{60} dimer have the same pattern as for $(C_{59}N)_2$ but are slightly down shifted except for the lowest frequency mode which is upshifted by 6 cm^{-1}. Values for the individual components are at 88, 98, and 106 cm^{-1} as listed in Table 1, column 7. With increasing temperature, the lowest and the highest component of the three lines become rather strong and disappear when the transition to the monomeric or polymeric phase is approached (not shown explicitly). This is in contrast to the behavior of the same lines in $(C_{59}N)_2$ which appear highly independent of temperature. The intercage modes of the single bonded dimers should be also related to the intercage modes of cyclobutane-bonded dimers or polymers as it is done in Table 1, columns 3 and 6. These modes appear throughout at higher frequencies as compared to the modes in the single bonded material.

Details of similarities and differences are evident from the comparison of the positions for the most characteristic modes listed in Table 1. The most striking difference is the position for the pentagonal pinch mode which appears at 1463 cm^{-1} for $(C_{59}N)_2$ and at 1451 cm^{-1} for $(C_{60}^-)_2$.

4 Discussion

The similarity for the intercage modes is an immediate consequence of the similarity between the geometric configurations summarized in Table 2. For all calculated distances the difference between $(C_{59}N)_2$ and $(C_{60}^-)_2$ is less than 1% except for the intercage separation. For the latter the difference amounts to more than 2% and the value for $(C_{59}N)_2$ is larger than the value for $(C_{60}^-)_2$. This is surprising on account of the much lower thermal stability observed for $(C_{60}^-)_2$ as compared to $(C_{59}N)_2$. It is, however, consistent with the higher value for the intercage stretching mode in $(C_{60}^-)_2$ as shown in Table 1, third line from the bottom. Concerning the stability one can conclude that the intercage bond is not the most important parameter for the stability. Obviously intercage bonds can be rather long and the dimer will still not dissociate if there is no low energy ground state for the dissociated geometry. This is the case for $(C_{59}N)_2$ where the bonds do not break until the cage itself degrades [23]. The described behavior is also consistent with the observation that in contrast to $(C_{60}^-)_2$, heating $(C_{59}N)_2$ does not yield spectra from monomeric species [23].

Calculated frequencies for the intercage modes are 85, 108, and 117 cm^{-1} for the C_{60} dimer and 88, 108, and 126 cm^{-1} for $(C_{59}N)_2$ and thus in very good agreement with the experiment in general. The normal coordinates indicate that the lowest frequencies correspond to the intercage stretching. This is in agreement with an analysis previously reported for the cyclobutane bonded dimer [24]. With this assignment the experimentally observed intercage stretching modes follow a trend as expected intuitively. For $(C_{59}N)_2$ which has the longest intercage bond the frequency is lowest. $(C_{60}^-)_2$ has a shorter intercage bond and thus a higher intercage frequency. Finally, $(C_{60})_2$ has two single intercage bonds and thus one expects the highest intercage frequency. Unfortunately the AM1 calculation does not reproduce this trend, at least not for the two single bonded dimeres as the value of 85 cm^{-1} calculated for $(C_{60}^-)_2$ is lower than the value of 88 cm^{-1} calculated for $(C_{59}N)_2$. The reason for this discrepancy may be due to the fact that the normal coordinates for this mode spreads out over a much wider region of the molecule than expected from the simplified picture of two cages vibrating against each other and therefore need a more sophisticated evaluation. This is consistent with a detailed local density approximation (LDA) based analysis of the vibrational species of the dimers [25].

The split off of the fifth component of the $H_g(1)$ derived band is also almost the same for the two dimeres analyzed here. It was also observed at about the same position in the cyclobutane bonded dimers. For longer ring bonded oligomers, the line was found by LDA calculations to shift up to 340 cm^{-1} [26,27]. It is one of the most significant features in the Raman spectra of this type of linear polymers. In the undoped or doped orthorhombic linear polymers this line is observed at 345 cm^{-1} [28].

The general agreement between the spectra of $(C_{59}N)_2$ and $(C_{60}^-)_2$ is relaxed with respect to several findings. The differences are small but obviously relevant for the differences in the electronic structure of the two dimers. The smaller line splitting and the narrower lines mentioned in Section 3 are indicative for a more homogeneous

distribution of the atomic potential in the C_{60} dimer. Both findings allow an even better correlation between the modes observed in $(C_{60}^-)_2$ and the modes of C_{60} than with those for $(C_{59}N)_2$.

Splittings due to the loss of degeneracy in $(C_{60}^-)_2$ scale roughly with the decrease of the radial component of the modes. Whereas the average splitting between the components for the modes $H_g(1)$ is about 8 cm^{-1} it is decreased to about 5 cm^{-1} for $H_g(2)$, to 3.5 cm^{-1} for $H_g(6)$ and unresolvable for $H_g(8)$.

The assignment is now rather consistent for the two dimers. Interestingly all G_g modes remain unsplit. This is independent of the amount of radial character. As a consequence the response from these modes appears as a very strong line. No physical interpretation is available for this phenomenon as yet. The few additional lines in the spectrum of $(C_{60}^-)_2$ which were not assigned to gerade modes are rather weak and may safely be correlated to modes derived from ungerade species of C_{60} or to sum and difference response from two or more gerade modes.

The similarity of the resonance behavior for the two dimers $(C_{59}N)_2$ and $(C_{60}^-)_2$ suggests similar optical absorption and a similar reason for its downshift. The downshift may be assigned formally to additional oscillator strength from a t_{1u}-t_{1g} derived transition, activated by the occupation of the t_{1u} state with the extra electrons from the nitrogens. Such interpretations must be considered with care, since the electrons either from the nitrogens in $(C_{59}N)_2$ or from the charge transfer in $(C_{60}^-)_2$ remain highly localized and their orbital energy might be rather different from an orbital energy of an electron in the t_{1u} derived level. From *ab initio* quantum-chemical calculations the energy levels are less split in $(C_{59}N)_2$ due to the extra Coulomb energy of the charged nitrogen on the cage [6]. The situation is simpler in the case of $(C_{60}^-)_2$ where no extra Coulomb potential exists and the molecular potentials are therefore more smooth.

The line position for the pentagonal pinch mode in the dimeric phases deserves also some attention. The values of 1451 cm^{-1} for the C_{60}^- dimer and 1463 cm^{-1} for the $C_{59}N$ dimer are dramatically different. In fact the former is considerably lower than expected whereas the latter is higher than expected. From columns 2 and 4 in Table 1 the values of the $A_g(2)$ mode for C_{60} and C_{60}^- exhibit the expected downshift of 7 cm^{-1} for the extra charge at high temperatures. For the down shift upon polymerization by the cyclobutane ring we find for the uncharged system 1467 $\rightarrow$ 1459 (8 cm^{-1}) and for the charged system 1457 (+3 from the reduction of temperature) $\rightarrow$ 1 454 (6 cm^{-1}). For the undoped dimer we find only a downshift of 4 cm^{-1}. This means consistently 3 or 4 cm^{-1} shift per extra ring bonding. Applying such estimates to the C_{60}^- dimer we obtain for temperatures of 270 K 1461 cm^{-1} for the monomer and 1457 cm^{-1} for the dimer. The latter value is in between the results observed for $(C_{60}^-)_2$ and $(C_{59}N)_2$ but still contrasts the values of (1451 cm^{-1}) and 1463 cm^{-1} from columns 7 and 8 in Table 1. The weaker bonding (longer intercage bond) may lead to a reduction of the influence of the intercage bond on the frequency of the pinch mode in $(C_{59}N)_2$ whereas less extended delocalization of the extra electron in $(C_{60}^-)_2$ (compared to a full delocalization in the monomeric A_xC_{60} compounds) may enhance the downshift of the mode. A detailed explanation for the unusual line positions for the pentagonal pinch mode remains, however, a challenge for a more sophisticated quantum-chemical calculation.

The transition from the quenched monomer of C_{60}^- to the dimer is rather sharp in temperature and well characterized by the appearance of the new Raman lines around 100 cm^{-1}, at 293, 513, and 623 cm^{-1}, by the downshift of the pentagonal pinch modes from 1 462 to 1 453 cm^{-1}, respectively, and by the sudden splitting of the modes $H_g(3)$ and $H_g(4)$ at a temperature above 130 and below 160 K. The definitive stability range of the dimeric phase may thus be located between 150 K and 260 K.

The above limits of stability can be compared to results from ESR and differential thermal analysis (DTA) [13]. Referring to the former a loss of the metallic state was observed at 125 K which was interpreted as the transition to the dimeric phase. The endothermic reaction assigned to the transition was, however, only observed at 200 K [13]. The high temperature edge for the stability was observed by both techniques at 270 K. Thus, at least the results for the high temperature stability limit are in very good agreement with our findings. For the low temperature stability limit the discrepancy between the ESR results and the results from DTA are removed in a sense that our observation is intermediate between the two previously reported values.

The dramatic change for the relative intensities of the modes at 513 cm^{-1} and at 293 cm^{-1} as depicted in Figure 6 is remarkable. As this change is for relative intensities, it must be taken seriously. Since for both modes the resonance transition is the same at any temperature the different response can only originate from a change of the electron-phonon coupling with temperature. Such changes indicate a considerable change in the normal coordinates of the modes and thus a considerable relaxation of the cage geometry which eventually leads to a fraction of the intercage bonds as discussed below.

Above about 260 K the new line appearing in the frequency range of the pinch mode and located at 1 458 cm^{-1} indicates another phase transition. The value observed for the frequency is a little lower than expected for a singly charged and unbonded C_{60} molecule but considering the lower temperature and some uncertainty in the exact value for the center of the line it is safely assigned to the response from the monomeric C_{60}^- species. Thus the dimer dissociates into a monomer before it finally connects to the ring bonded phase. This dissociation is indeed a request to establish a bonding by the cyclo addition reaction as the latter needs free rotation of the cages. The existence of the intermediate phase is restricted to a very narrow temperature range. It may even be that the monomeric state is indeed only a local transient to the orthorhombic polymeric phase. Comparing to the results from ESR and DTA the agreement is again rather good. In the latter experiments the transition to the monomeric phase was

observed at 270 K and the stability range for this phase was rather narrow, only 30 K [13]. In contrast, the stability range for the monomeric phase in CsC_{60} is much larger. It extends from 220 to 270 K [13,14].

5 Conclusion

In conclusion we demonstrated the strong relation between the Raman response of the isostructural and isoelectronic fullerene dimers $(C_{59}N)_2$ and $(C_{60}^-)_2$). Both compounds exhibit a splitting of degenerate modes and a strong resonance for excitation with red lasers. At least for the biazafullerene this resonance is consistent with the downshift of the optical absorption edge as compared to C_{60}. The splitting in $(C_{60}^-)_2$ is stronger for the radial modes as compared to the tangential modes.

A more detailed comparison reveals several differences between the two materials. For $(C_{59}N)_2$ X-ray data and semi-empirical quantum-chemical calculations reveal a larger intercage bond length, the Raman lines are broader, and the splitting is larger. These results are traced back to the less uniform molecular potentials in the heterofullerene dimers as compared to the homofullerene dimers.

The various phases which appear during the annealing process of the $(C_{60}^-)_2$ were analyzed. The monomeric phase following the dimeric structure was observed as a transient structure at 270 K. Even though this structure is definitely observed, an extended stability range could not be located on the temperature scale.

Assignment of the Raman lines observed for $(C_{60}^-)_2$ could be performed with an unprecedented quality if C_{60} was taken as a reference material. Whereas the former H_g and F_g modes exhibited the expected splitting the G_g derived modes remained unsplit and of accordingly high intensity.

Valuable discussions with M. Krause and S. Stafstroem are greatly acknowledged. Work supported by the European Community, TMR project ERBFMRX-CT97-0155 and by the FFWF in Austria, project P11943. T.P. acknowledges an APART fellowship of the Austrian Academy of Sciences. N.T. also thanks the European Community for a Marie Curie Fellowship at the University of Sussex.

References

1. J.C. Hummelen *et al.*, Science **269**, 1554 (1995).
2. A. Lahamer *et al.*, Adv. Metal Semicond. Clust. **4**, 179 (1998).
3. M. Keshavarz-K *et al.*, Nature **383**, 147 (1996).
4. C.M. Brown *et al.*, J. Am. Chem. Soc. **118**, 8715 (1996).
5. W. Andreoni, Ann. Rev. Phys. Chem. **49**, 405 (1998).
6. T. Pichler *et al.*, Phys. Rev. Lett. **78**, 4249 (1997).
7. S. Haffner *et al.*, Eur. Phys. J. B **1**, 11 (1998).
8. J. Winter, H. Kuzmany, Solid State Commun. **84**, 935 (1992).
9. Q. Zhu *et al.*, Phys. Rev. B **47**, 13948 (1993).
10. P. Stephens *et al.*, Nature **370**, 636 (1996).
11. H. Kuzmany *et al.*, *Physics and Chemistry of Fullerenes*, edited by K. Prassides (Kluwer Academic Pub., 1994), p. 287.
12. A. Lappas *et al.*, J. Am. Chem. Soc. **117**, 7560 (1995).
13. M. Kosaka *et al.*, Phys. Rev. B **51**, 12018 (1995).
14. L. Granasy, S. Pekker, L. Forro, Phys. Rev. B **53**, 5059 (1996).
15. G. Oszlanyi *et al.*, Phys. Rev. B **51**, 12228 (1995).
16. J. Kürti, K. Nemeth, Chem. Phys. Lett. **256**, 119 (1996).
17. G. Oszlanyi *et al.*, Phys. Rev. B **54**, 11849 (1996).
18. H. Kuzmany *et al.*, Phys. Rev. B **60**, 1005 (1999).
19. S. Lebedkin *et al.*, Chem. Phys. Lett. **285**, 210 (1998).
20. B. Burger, Thesis, University of Vienna, 1998.
21. B. Burger, J. Winter, H. Kuzmany, Z. Phys. B **101**, 277 (1996).
22. J. Winter *et al.*, Phys. Rev. B **54**, 17486 (1996).
23. M. Krause *et al.* (unpublished).
24. H.J. Eisler *et al.*, J. Phys. Chem. A **102**, 3889 (1998).
25. W. Andreoni, A. Curioni, private communication.
26. D. Porezag *et al.*, Phys. Rev. B **52**, 14963.
27. J. Winter, H. Kuzmany, Carbon **36**, 599 (1998).
28. J. Winter, H. Kuzmany, Phys. Rev. B **52**, 7115 (1995).